Transport and fractionation in periodic potential-energy landscapes

Matthew Pelton and Kosta Ladavac
Department of Physics and James Franck Institute, The University of Chicago, Chicago, Illinois 60637, USA

David G. Grier
Department of Physics and Center for Soft Matter Research, New York University, New York, New York 10003, USA

(Received 9 April 2004; published 24 September 2004)

Objects driven through periodically modulated potential-energy landscapes in two dimensions can become locked in to symmetry-selected directions that are independent of the driving force's orientation. We investigate this problem in the overdamped limit, and demonstrate that the crossover from free-flowing to locked-in transport can depend exponentially on an object's size, with this exceptional selectivity emerging from the landscape's periodicity.

DOI: 10.1103/PhysRevE.70.031108 PACS number(s): 05.60.Cd, 81.20.Ym, 82.70.−y

I. INTRODUCTION

The theme of transport through modulated potential-energy landscapes pervades solid-state physics and arises in many natural and industrial processes. This problem has been studied extensively in the quantum-mechanical limit. Considerably less attention has been paid to the classical limit, where effects such as viscous damping and thermal randomization complicate the analysis. This article focuses on noninertial transport of classical objects driven through periodically modulated potential-energy landscapes by constant, uniform forces. The one-dimensional variant of this problem has been thoroughly investigated [1], and its results have been applied profitably to such processes as gel electrophoresis. We focus instead on the overdamped motions of classical objects as they flow through two-dimensional periodic landscapes, about which far less is known. Such higher-dimensional periodic landscapes have shown exceptional promise as a mechanism for sorting mesoscopic objects. Our discussion draws upon recent experimental realizations of this process in which macromolecules or mesoscopic colloidal particles are observed while moving through arrays of microfabricated posts [2,3] and through regular arrays of optical traps [4–6]. In both cases, particles' differing interactions with the physical landscape and their differing responses to the external driving force can cause them to follow radically different paths, and thus into distinct fractions.

Section II introduces the theoretical framework for describing driven objects' interactions with inhomogeneous environments in the context of recent experimental realizations. We then apply this in Sec. III to the particularly simple case of transport across a linear barrier or potential trench. Such a landscape can continuously sort mixtures of objects into two distinct fractions, but with only algebraic sensitivity to properties such as size. Generalizing to periodic landscapes in Secs. IV and V leads generally to fractionation with *exponential* size selectivity. Exploiting this exceptional resolution for practical separations may be difficult, however, in the most straightforward implementations. Other potential landscapes, such as a line of discrete potential wells, discussed in Sec. VI, offer exponential size selectivity with good prospects for practical implementations.

II. MOTIONS THROUGH LANDSCAPES

A. The equation of motion

Consider a Brownian particle moving, under the influence of a uniform driving force $\mathbf{F}_0$, through the force field $\mathbf{F}(\mathbf{r})$ due to an inhomogeneous medium or landscape. Its trajectory is described by the Langevin equation [1,7]

$$\xi\frac{d\mathbf{r}}{dt} = \mathbf{F}(\mathbf{r}) + \mathbf{F}_0 + \mathbf{\Gamma}(t), \tag{1}$$

where ξ is the particle's viscous drag coefficient, and $\mathbf{\Gamma}$ describes random thermal fluctuations. This Langevin force satisfies $\langle\mathbf{\Gamma}(t)\rangle = \mathbf{0}$ and $\langle\mathbf{\Gamma}(t)\cdot\mathbf{\Gamma}(t+\tau)\rangle = \xi\, k_B T\, \delta(\tau)$ at temperature T, where $\delta(\tau)$ is the Dirac delta function. A sphere of radius a immersed in an unbounded fluid of viscosity η, for example, has $\xi = 6\pi\eta a$.

In the limit that $\mathbf{F}_0$ and $\mathbf{F}$ both greatly exceed the scale of thermal forces $\mathbf{\Gamma}$, the Langevin equation, Eq. (1), reduces to a first-order deterministic equation of motion. This article focuses on two-dimensional systems, the simplest case exhibiting nontrivial behavior. Even this deceptively simple system yields surprising results, as we will see.

B. The driving force

In the particular case of fluid-borne colloidal particles, a uniform driving force might be exerted by viscous drag, by gravity, or through electrophoresis, magnetophoresis, or thermophoresis. Each of these plays a central role in practical fractionation techniques [8]. More generally, analogous results should be expected for such related systems as electrons flowing through a periodically gated low-mobility two-dimensional electron gas [9], magnetic flux quanta creeping through patterned type-II superconductors [10–12] or Josephson junction arrays [13], and atoms migrating across crystal surfaces [14].

In some instances of practical interest, the driving force itself can be modulated by the physical landscape, leading to additional interesting effects [15]. These, however, are beyond the scope of the present discussion. Time-dependent driving forces also lead to exciting phenomena, but are not

required for the effects we describe. We consider the simplest case, where the driving force $\mathbf{F}_0$ is both uniform and constant and is oriented at a fixed angle θ with respect to the landscape symmetry axis, here denoted $\hat{x}$.

In the absence of other influences, particles would travel along the driving direction while dispersing diffusively in the transverse direction. Differential dispersion by transverse diffusion has proved useful for continuously fractionating heterogeneous samples across laminar flows in microfluidic channels [16]. Adding a modulated substrate opens up additional avenues for separating particles according to their sizes, and can greatly improve the resolution of such separations.

C. Creating landscapes

Several approaches have been introduced in recent years for structuring potential-energy landscapes on molecular, macromolecular, and cellular lengths scales. Among these are arrays of lithographically defined microscopic posts integrated into hermetically sealed fluidic channels, which provide a periodic and precisely tuned alternative to the gels used for electrophoresis [17]. Arrays of interdigitated electrodes [18,19] have also been used to establish periodic potentials through dielectrophoresis. The emphasis in these studies, however, has been on ratchetlike behavior induced by time-dependent potentials.

More recently, techniques have been developed for tailoring extensive potential-energy landscapes using forces exerted by light. The most capable of these exploit optical gradient forces, meaning that dipole moments induced in illuminated objects respond to gradients in the light's electric field. Such forces are the basis for the single-beam optical trap known as an optical tweezer [20], which acts as a potential-energy well for particles with appropriate optical properties. More generally, an extended optical intensity distribution will produce an associated potential-energy landscape.

The most straightforward way to project periodic intensity profiles is to create a standing-wave interference pattern from two or more coherent beams of light. Such patterns have come to be known as optical lattices, particularly when applied to controlling the distributions and motions of matter. More general intensity patterns can be created with holographic optical tweezers [21–23] or with the generalized phase contrast technique [24], which establish extended optical trapping patterns using computer-generated holograms.

D. Form factors

The physical landscape may be represented by a function $I(\mathbf{r})$ describing a potential-determining property such as the local optical intensity. An object's potential energy at $\mathbf{r}$ is not simply proportional to $I(\mathbf{r})$, but depends on the object's geometry and composition. For example, larger particles approaching a well-localized optical trap encounter the trap's intensity gradients at larger ranges than smaller particles. The observation that different objects passing through the same environment experience different potential-energy landscapes provides the foundation for the results that follow.

The effective potential may be expressed as the convolution,

$$V(\mathbf{r}) = (f \circ I)(\mathbf{r}) \tag{2}$$

$$= \int f(\mathbf{x}-\mathbf{r}) I(\mathbf{x}) d^2x, \tag{3}$$

of the two-dimensional landscape $I(\mathbf{r})$ with a form factor $f(\mathbf{r})$ describing the object's interaction with the landscape. In comparing to experimental realizations, we assume that contributions from the form factor's third dimension have been integrated out. If $I(\mathbf{r})$ has a symmetry axis along the $\hat{x}$ direction, then the associated force

$$\mathbf{F}(\mathbf{r}) = -\nabla (f \circ I)(\mathbf{r}) \tag{4}$$

generally does as well. Convolving with $f(\mathbf{r})$ broadens features in $I(\mathbf{r})$ by an amount that depends on the object's size, shape, orientation, and composition.

In many cases of practical interest, the convolution in Eq. (2) is most easily performed using the Fourier convolution theorem:

$$(f \circ I)(\mathbf{r}) = \mathcal{F}^{-1}\{\tilde{f}(\mathbf{k})\tilde{I}(\mathbf{k})\}, \tag{5}$$

where $\tilde{f}(\mathbf{k})$ and $\tilde{I}(\mathbf{k})$ are the Fourier transforms of $f(\mathbf{r})$ and $I(\mathbf{r})$, respectively, and $g(\mathbf{r}) = \mathcal{F}^{-1}\{\tilde{g}(\mathbf{k})\}$ denotes the inverse Fourier transform of $\tilde{g}(\mathbf{k})$. In some particularly simple cases, both $\tilde{f}(\mathbf{k})$ and $\tilde{I}(\mathbf{k})$ can be factored into components along the $\hat{x}$ and $\hat{y}$ directions, reducing Eq. (5) to a product of one-dimensional integrals. In other cases, separable approximations for the form factor emerge as the leading-order cumulant expansion of $\tilde{f}(\mathbf{k})$.

For example, the form factor for a uniform dielectric cube of side a aligned with the x axis and illuminated by collimated light is

$$f(\mathbf{r}) = \alpha a \, \Theta\left(\frac{a}{2} - |x|\right)\Theta\left(\frac{a}{2} - |y|\right), \tag{6}$$

where $\Theta(x)$ is the Heaviside step function, and

$$\alpha = 2\pi \frac{\sqrt{\epsilon_0}}{c}\left(\frac{\epsilon_0 - \epsilon}{\epsilon + 2\epsilon_0}\right) \tag{7}$$

describes the matter-light interaction, in the quasistatic limit, for a material of dielectric constant ϵ immersed in a medium of dielectric constant ϵ_0 [25]. Both this geometry and the collimated light field are far simpler than would be encountered in most real-world optical trapping implementations [26], but serve to illustrate our approach. A more complete treatment of optical forces would also incorporate polarization effects, which cannot be captured in the present scalar theory. Higher-order effects such as Mie resonances [25] could be taken into account through α, but will be ignored in the current discussion. Note that α is negative for a high-dielectric-constant material in a low-dielectric-constant medium; such particles are drawn toward regions of high intensity. Low-dielectric-constant particles, by contrast, are repelled by light.

The aligned cube's form factor is separable, with Fourier transform

$$\tilde{f}(\mathbf{k}) = \alpha\, a^3\, \tilde{f}_x(k_x a)\tilde{f}_y(k_y a). \tag{8}$$

The individual components are readily shown to be

$$\tilde{f}_x(ka) = \tilde{f}_y(ka) = \frac{\sin ka}{ka}. \tag{9}$$

Their leading-order cumulant expansion

$$\tilde{f}_x(ka) = \tilde{f}_y(ka) \approx \exp\left(-\frac{1}{6}k^2a^2\right) \tag{10}$$

for $ka < \pi$ demonstrates that the form factor's Fourier transform depends sensitively on particle size for a given wave number. Note that, as defined, $\tilde{f}_x(ka)$ and $\tilde{f}_y(ka)$ are dimensionless and normalized to unity at $ka=0$.

The form factor for a uniform dielectric sphere of radius a illuminated by collimated light of wavelength $\lambda > a$ is [25]

$$f(\mathbf{r}) = \alpha\, \sqrt{a^2 - r^2}\, \Theta(a-r), \tag{11}$$

which is not separable. The leading-order cumulant expansion of $\tilde{f}(\mathbf{k})$, however, is separable, with

$$\tilde{f}(\mathbf{k}) \approx \alpha\frac{2\pi a^3}{3}\tilde{f}_x(k_x a)\tilde{f}_y(k_y a), \tag{12}$$

where

$$\tilde{f}_x(ka) = \tilde{f}_y(ka) = \exp\left(-\frac{1}{10}k^2a^2\right) \tag{13}$$

for $ka < 8$.

More generally, an object's form factor is nonzero only over a limited domain set by its size. The corresponding Fourier transform thus depends strongly on ka, within the appropriate range of wave numbers. We capture the ramifications of this boundedness by adopting the separable Gaussian form

$$f(\mathbf{r}) = \alpha\, a\, \exp\left(-\frac{r^2}{2a^2}\right), \tag{14}$$

whose Fourier transform

$$\tilde{f}(\mathbf{k}) = 2\pi\alpha a^3\, \tilde{f}_x(k_x a)\tilde{f}_y(k_y a) \tag{15}$$

has components

$$\tilde{f}_x(ka) = \tilde{f}_y(ka) = \exp\left(-\frac{1}{2}k^2a^2\right). \tag{16}$$

Landscape $I(\mathbf{r})$ determines which wave numbers contribute to the object's transport properties. The following sections explore a few particularly effective choices.

III. LINEAR FRINGES

In part to motivate a discussion of periodic potential-energy landscapes, we first consider how objects traverse a single trench or barrier arranged at an angle to the driving force. This kind of landscape may be realized, for example, by creating a linear optical trap with a cylindrical lens or a diffractive line generator. Because such an optical landscape can act as either a barrier or a trench, depending on the sign of α, we will refer to both as fringes. In either case, a fringe aligned with the $\hat{x}$ axis inhibits transport in the transverse direction. We model such a landscape as a Gaussian profile of intrinsic width w,

$$I(\mathbf{r}) = I_0\, \exp\left(-\frac{y^2}{2w^2}\right). \tag{17}$$

Using the object's form factor as defined in Eq. (14), the associated potential is

$$V(\mathbf{r}) = 2\pi\alpha I_0 \frac{a^3 w}{\sigma(a)}\exp\left(-\frac{y^2}{2\sigma^2(a)}\right). \tag{18}$$

The fringe's apparent width to a particle of size a is broadened to $\sigma(a) = \sqrt{a^2 + w^2}$.

In the limit that thermal forces may be ignored, the equations of motion reduce to the deterministic form

$$\frac{dx}{dt} = v_0 \cos\,\theta, \tag{19}$$

$$\frac{dy}{dt} = \xi^{-1}\, F_y(y) + v_0 \sin\,\theta, \tag{20}$$

where the landscape-free drift speed is $v_0 = \xi^{-1}F_0$ and

$$F_y(y) = 2\pi\,\alpha I_0 \frac{a^3 w}{\sigma^3(a)} y\, \exp\left(-\frac{y^2}{2\sigma^2(a)}\right). \tag{21}$$

The landscape's restoring force $F_y(y)$ reaches a maximum at a distance $y = y_{\max}$ from the fringe's axis, with $y_{\max} = \sigma(a)$ for our particular example. If $F_0 \sin\,\theta > F_y(y_{\max})$ then a particle can cross the barrier. Such particles may be said to *escape* the barrier. By contrast, particles for which the barrier is insurmountable travel unimpeded along the $\hat{x}$ direction at speed $v_x = v_0 \cos\,\theta$ and are said to be *locked into* the landscape.

The marginal angle θ_m at which an object just barely remains locked into the barrier determines which objects are deflected and which are not. The dependence of θ_m on particle size and other characteristics establishes the sensitivity of the sorting technique. Referring to Eqs. (20) and (21), the condition for locked-in transport,

$$\sin\,\theta \leqslant \sin\,\theta_m \equiv \frac{F_y(y_{\max})}{F_0} \tag{22}$$

$$= \frac{|\alpha| I_0}{F_0}\frac{2\pi}{\sqrt{e}}\frac{a^3 w}{a^2 + w^2}, \tag{23}$$

applies to both attractive trenches ($y_{\max} = +\sigma$) and repulsive barriers ($y_{\max} = -\sigma$). The general result Eq. (22) applies even if $f(\mathbf{r})$ is not separable because, in this case at least, $I(\mathbf{r})$ is independent of x.

The particular result in Eq. (23) shows than the marginal lock-in angle depends only algebraically on size, and only linearly on other properties through α. This is neither better nor worse than the performance offered by other established techniques such as gel electrophoresis or flow-field fractionation [8]. One substantial benefit offered by selective transport across a fringe is its ability to process a continuous stream of objects rather than being restricted to discrete batches. The selected fraction, moreover, can be tuned continuously, for example, by adjusting I_0, F_0, w, or θ. Optical implementations also can be optimized by varying the wavelength of light, in which case resonances might be exploited as a complementary mechanism for size separation.

Although a single fringe's performance is somewhat lackluster, one might expect multiple fringes to fare better. The first step along this direction is to consider a pair of parallel Gaussian fringes. The effective potential is the sum of two single-fringe potentials:

$$V(\mathbf{r}) = 2\pi\alpha I_0 \frac{a^3 w}{\sigma(a)} \left[\exp\left(-\frac{(y+b/2)^2}{2\sigma^2} \right) + \exp\left(-\frac{(y-b/2)^2}{2\sigma^2} \right) \right], \tag{24}$$

where b is the fringe separation. If $b < \sigma$, the two fringes overlap enough that the landscape resembles a single, broadened fringe. Again, no more than algebraic selectivity should be expected. In the opposite limit, $b \gg \sigma$, the fringes are independent, and particles cross the double barrier with the same facility with which they cross one. Neither of these cases offers benefits over the single fringe.

For intermediate b, on the other hand, the landscape consists of two unequal barriers, the smaller of which lies between the two fringes. The smaller barrier's height depends strongly on b/σ, which, in turn, depends on the particle size a. This lower intermediate barrier does not affect the fringes' overall ability to separate objects, which is dominated by the larger barrier. It suggests the possibility, however, that transport across N overlapping fringes could be highly sensitive to particle size. Those particles not able to jump the interfringe barriers will be locked in and swept aside while others will hop from one fringe to the next across the field. Highly selective sorting is thus possible if edge effects due to the first or last fringe (in the case of trenches or barriers, respectively) can be circumvented.

IV. SINUSOIDAL LANDSCAPES

The foregoing discussion suggests that a periodically modulated landscape inclined at an angle to the driving force might be more effective than a single fringe at sorting objects by size. To make this more concrete, and to illuminate the role of periodicity, we consider the simplest and most instructive example of such a landscape, a sinusoid in the $\hat{y}$ direction:

$$I(\mathbf{r}) = I_0 \cos(k_0 y), \tag{25}$$

shown schematically in Fig. 1. Apart from its mathematical simplicity, this landscape has the advantage of being readily

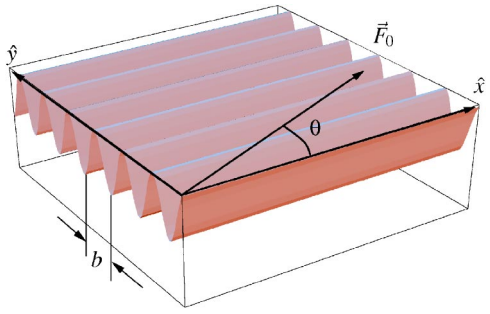

FIG. 1. Schematic representation of a sinusoidal landscape, modulated along the $\hat{y}$ direction.

implemented experimentally. In the case of optical forces, a sinusoidal pattern can be created by interfering two coherent laser beams, with the wave number k_0 being determined by the optical wavelength and the angle between the beams. Such an interference pattern is known as a one-dimensional optical lattice [27], and is commonly used to control and distribute cold atoms. More recently, optical lattices have been used to separate populations of colloidal particles on the basis of their sizes and indices of refraction [5].

The key to such a potential's efficacy is in its Fourier transform:

$$\tilde{I}(\mathbf{k}) = (2\pi)^2 I_0 \delta(k_x)\delta(k_y - k_0). \tag{26}$$

Convolution according to Eq. (5) therefore picks out the component of the form factor's Fourier transform at wave number k_0:

$$V(\mathbf{r}) = I_0 \int \tilde{f}(\mathbf{k})\delta(k_x)\delta(k_y - k_0)\cos(k_x x)\cos(k_y y) d^2k \tag{27}$$

$$= I_0 \tilde{f}(0, k_0)\cos(k_0 y). \tag{28}$$

Assuming a separable form for $\tilde{f}(\mathbf{k})$ such as Eq. (16),

$$V(\mathbf{r}) = I_0 \tilde{f}_y(k_0 a)\cos(k_0 y) \tag{29}$$

$$= \alpha\sqrt{2\pi} I_0 a^3 \exp\left(-\frac{1}{2} k_0^2 a^2 \right) \cos(k_0 y). \tag{30}$$

For particle sizes satisfying $k_0 a > \sqrt{3}$, the amplitude of the potential energy landscape's sinusoidal modulations now depends strongly on particle size through the wave number dependence of the form factor. The particular form in Eq. (30) reflects our choice of a Gaussian form factor in Eq. (14). However, the arguments leading to this choice reveal that comparable results should be obtained quite generally for particles whose size is smaller than the wavelength of the physical landscape's undulations (e.g., for spherical particles satisfying $k_0 a < 8$).

A. Deterministic limit

A particle's trajectory through the sinusoidal landscape is described in the deterministic limit by Eqs. (19) and (20), with

$$F_y(y) = \alpha\sqrt{2\pi} I_0 k_0 a^3 \exp\left(-\frac{1}{2}k_0^2 a^2\right)\sin(k_0 y). \quad (31)$$

Nonseparable form factors again yield similar results, because $I(\mathbf{r})$ is independent of x. Because $\sin(k_0 y) \leqslant 1$, particles become locked into the $\hat{x}$ direction for orientations satisfying

$$\sin\,\theta \leqslant \sin\,\theta_m = \frac{|\alpha| I_0}{F_0}\sqrt{2\pi} k_0 a^3 \exp\left(-\frac{1}{2}k_0^2 a^2\right). \quad (32)$$

By contrast to Eq. (23), this reflects an exceptional sorting sensitivity: whether or not a particle becomes entrained by the fringes depends *exponentially* on particle size for $k_0 a > 1$. Among established fractionation schemes, only affinity chromatography offers comparable selectivity [8], and this can operate only on discrete samples of a limited class of macromolecules. Fractionation in a sinusoidal landscape can operate on continuous sample streams and can be implemented for a wide range of sample types.

Equations (19), (20), and (30) can be directly integrated for this simple landscape. The motion in the $\hat{x}$ direction is trivial:

$$x(t) = v_0 \cos\,\theta\, t. \quad (33)$$

If the particles are locked in [i.e., if Eq. (32) is satisfied], then the particles make no progress in the $\hat{y}$ direction, and $y(t)$ is constant. Otherwise, integration gives

$$y(t) = \frac{2}{k_0}\arctan\left[\sqrt{\frac{\sin\,\theta + \eta}{\sin\,\theta - \eta}}\tan\left(\frac{k_0 v_0 t}{2}\sqrt{\sin^2\theta - \eta^2}\right)\right], \quad (34)$$

where the relative strength of the landscape's modulation is

$$\eta(a) = \frac{I_0\, k_0 \tilde{f}(0, k_0 a)}{F_0}. \quad (35)$$

The time required to advance one fringe spacing $b = 2\pi/k_0$ can be seen to be

$$T = \frac{2\pi}{k_0 v_0 \sqrt{\sin^2\theta - \eta^2}}, \quad (36)$$

which yields a mean velocity in the $\hat{y}$ direction of

$$\langle v_y \rangle = v_0 \sqrt{\sin^2\theta - \eta^2}. \quad (37)$$

On average, the particle travels at an angle ψ to the $\hat{x}$ axis, given by

$$\tan\,\psi = \frac{\langle v_y \rangle}{\langle v_x \rangle} = \begin{cases} 0, & \sin\,\theta < \eta, \\ \dfrac{\sqrt{\sin^2\theta - \eta^2}}{\cos\,\theta}, & \sin\,\theta > \eta. \end{cases} \quad (38)$$

The deflection angle is plotted in Fig. 2(a) as a function of the driving force's orientation θ for various values of the normalized potential $\eta(a)$. The direction in which particles flow increases from $\psi = 0$ as the driving force's orientation crosses the condition for marginal lock-in, $\theta_m = \arcsin\,\eta$. At steeper angles, ψ approaches θ.

While this result is quite general, we can make the dependence on particle size more explicit by assuming the following functional form for $\eta(a)$, implied by Eqs. (14) and (35):

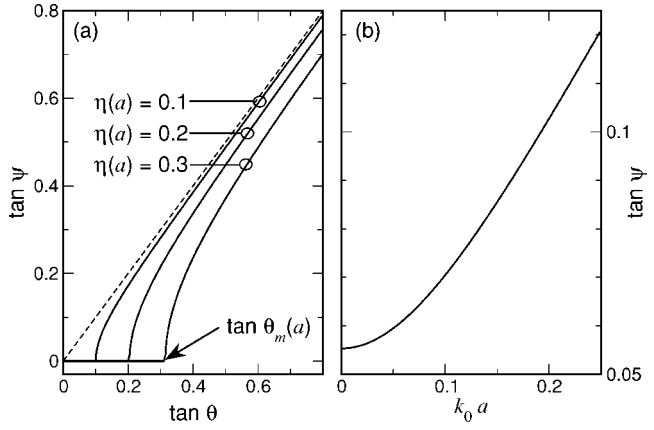

FIG. 2. (a) Travel direction for an inclined sinusoidal landscape as a function of orientation for fixed size and $\eta(a) = 0.1$, 0.2, and 0.3. Trajectories are locked in to $\psi(\theta) = 0$ for $\theta \leqslant \theta_m$. The diagonal dashed line indicates the result with no landscape. (b) Deflection angle as a function of particle size a at fixed driving orientation $\tan\,\theta = 0.441$, assuming $\eta_0 = 0.4$, independent of a.

$$\eta(a) = \eta_0 \exp\left(-\frac{1}{2}k_0^2 a^2\right), \quad (39)$$

where $\eta_0 = 2\pi\alpha a^3 I_0 k_0 / F_0$. Figure 2(b) shows the resulting dependence of deflection angle on particle size, if we assume that the driving and trapping forces are adjusted such that η_0 is a constant, independent of a. It can be seen that particles which are not locked in to the fringes at $\psi(a) = 0$ are fanned out into various directions, depending on their size.

Unlike the case of the single fringe, where a particle either flows along the fringe or else travels in the driving direction, the sinusoidal landscape's continuous dispersion distributes heterogeneous samples into multiple fractions, but also limits the achievable size resolution. The fraction dispersed into a finite angular range $\Delta\psi$ around ψ includes an associated range of sizes

$$\Delta a \approx \left(\frac{\partial \psi}{\partial a}\right)^{-1} \Delta\psi, \quad (40)$$

which, for the locked-in fraction at $\psi = \Delta\psi/2 \ll 1$, is

$$\Delta a \approx \cos^2\,\theta \left(\frac{\partial \eta^2}{\partial a}\right)^{-1} \Delta\psi^2. \quad (41)$$

Thus, the exponential size selectivity implied by Eq. (32) can be lost in the exponentially wide collection window imposed by $\eta(a)$ on practical implementations. This performance cannot be improved by passing the set of particles through the fringes a second time, because of the fixed relationship between Δa and $\Delta\psi$.

Although single-stage fractionation by a sinusoidal landscape yields broad size distributions, a narrow range of particle sizes can still be captured by using the following, two-step process. The deflection angle is first set such that all particles larger than a certain size a_2 will be locked in. These locked-in particles are discarded, and the remaining particles

are sent through a second potential landscape, with a different deflection angle, chosen such that all particles larger than a second size $a_1 < a_2$ are locked in. Only the locked-in particles from this second stage are then retained, so that all of the remaining particles have sizes in the range $[a_1, a_2]$, which can be made as small as desired.

With periodicity providing the essential ingredient for achieving exponential size selectivity, it might be expected that any periodic landscape would do. Unfortunately, this is not necessarily so. We already have demonstrated in Sec. III that an array of well-separated Gaussian fringes offers only algebraic, rather than exponential, size selectivity. A more general periodic landscape with wavelength $2\pi/k_0$ can be expanded as a Fourier series:

$$I(\mathbf{r}) = I_0 \sum_{n=0}^{\infty} \beta_n \sin(nk_0 y), \tag{42}$$

with Fourier coefficients β_n. If one of these coefficients is significantly larger than all the others, then the equations of motion can be approximated by Eqs. (19) and (20), and equivalently good size selectivity will be obtained. If, on the other hand, no single component dominates, then the superposition will not necessarily perform so well.

B. Biased diffusion

Modeling thermal effects is reasonably straightforward for the sinusoidal landscape. In this case, the Langevin equation [Eq. (1)] is most readily solved by transforming it into a Fokker-Planck equation for the probability density $\rho(\mathbf{r},t)$ of finding particles at position $\mathbf{r}$ at time t. If inertial effects are negligible, the Fokker-Planck equation for motion transverse to the fringes reduces to a Smoluchowski equation [1],

$$\partial_t \rho(y,t) + \partial_y S(y,t) = 0, \tag{43}$$

where the probability current is

$$S(y,t) = \xi^{-1}[F(r) - k_B T \partial_y]\rho(y,t). \tag{44}$$

In this equation, $F(r)$ is the total force on the particle, including the driving force and the force due to the potential landscape, T is the temperature, and k_B is Boltzmann's constant.

Following Ref. [1], Eq. (43) can be solved in the steady-state limit by taking $S(y,t) = S(y)$, independent of t. The resulting average drift velocity $\langle v_y \rangle$ for the sinusoidal potential of Eq. (30) is given by

$$\frac{\langle v_y \rangle}{v_0 \sin\theta} = 1 + \frac{2\sin\theta}{\eta} \mathrm{Im}\left[S_1\left(\tau, \frac{\sin\theta}{\eta}\right)\right], \tag{45}$$

where, as before, $\eta = k_0 I_0 \tilde{f}(0, k_0 a)/F_0$, and we have introduced the normalized temperature $\tau = k_B T/V_0$. The function $S_1(\tau, x)$ is defined recursively in terms of a continued-fraction expansion,

$$S_n(\tau,x) = \frac{1/4}{\tau + in\,x + S_{n+1}(\tau,x)}, \tag{46}$$

which converges rapidly with increasing order n.

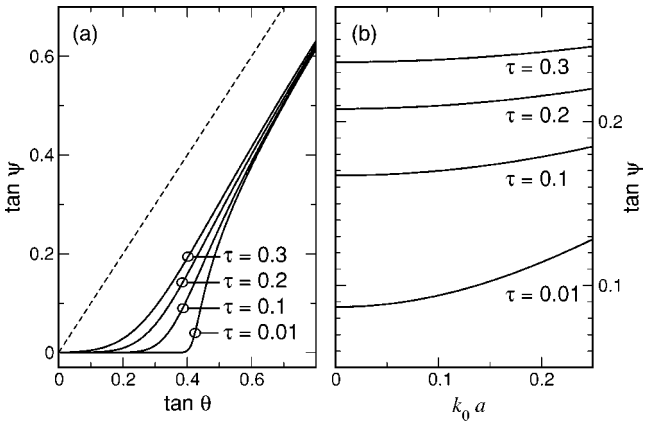

FIG. 3. (a) Deflection as a function of orientation at finite temperatures $\tau = 0.01$, 0.1, 0.2, and 0.3, assuming $\eta = 0.4$. The diagonal dashed line indicates the result with no landscape. (b) Dependence of the travel direction on particle size a for $\eta_0 = 0.4$, $\tan\theta = 0.441$, and the same set of temperatures. Raising the temperature weakens the size dependence of $\psi(a)$, and thus reduces the selectivity.

The average velocity in the $\hat{x}$ direction is unchanged from the zero-temperature case. The mean deflection angle ψ is thus given by

$$\tan\psi = \tan\theta \left\{ 1 + \frac{2\sin\theta}{\eta} \mathrm{Im}\left[S_1\left(\tau, \frac{\sin\theta}{\eta}\right)\right]\right\}. \tag{47}$$

This is plotted in Fig. 3(a) as a function of the angle θ of the driving force, for a fixed value of the normalized potential $\eta(a)$, and for various values of the normalized temperature τ. It can be seen that the effect of increasing temperature is to smooth out the transition between the locked-in and freely flowing states of motion. In the zero-temperature limit, the deflection angle is zero for all angles $\theta < \arcsin\eta$. For finite temperatures, the mean deflection angle is nonzero even in this "locked-in" state: the particles have a finite probability per unit time of being driven over the interfringe barrier by thermal fluctuations, and thereby advancing in the $\hat{y}$ direction.

The benefits of operating in the deterministic regime, in which thermal forces are negligible, can be seen in Fig. 3(b), where the deflection angle is shown as a function of the particle size a, for a fixed orientation θ, over a range of temperatures. Contrary to previous assertions that thermal effects can enhance size selectivity [5], the only effect of thermally assisted hopping in this system is to diminish the sorting resolution.

In other words, achieving high-sensitivity sorting in practice will require that the thermal energy scale be small compared to the landscape's modulation. In a real-world implementation, increasing the depth of modulation I_0 of the physical landscape will often be more practical than decreasing the temperature. Retaining the same lock-in conditions then requires that the driving force F_0 be increased proportionately. The practical limit on the achievable sorting efficiency will then be set by the maximum driving force or depth of modulation that can be obtained. For example, the

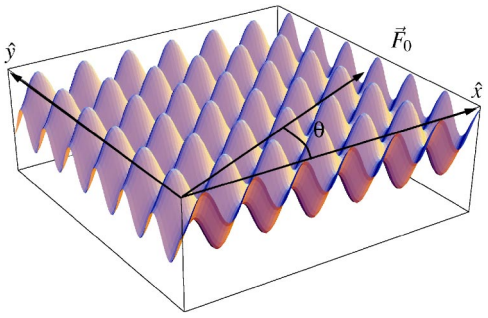

FIG. 4. Schematic representation of landscape sinusoidally modulated in both the $\hat{x}$ and $\hat{y}$ directions according to Eq. (48).

limitation for an optically implemented landscape is the available laser power.

V. SEPARABLE TWO-DIMENSIONAL LANDSCAPES

The one-dimensional potential of Eq. (25) is one of the few landscapes that allows for exact solutions of the equations of motion. Two-dimensional landscapes can be solved analytically only if the potential can be written as a sum of modulations in the $\hat{x}$ and $\hat{y}$ directions. In particular, we can consider separate sinusoidal modulation with the same period in the two directions:

$$I(\mathbf{r}) = I_0[\sin(k_0 y) + \sin(k_0 x)], \tag{48}$$

shown schematically in Fig. 4. This landscape is interesting mainly because it leads to decoupled equations of motion:

$$\frac{dx}{dt} = \xi^{-1} V_0 k_0 \cos(k_0 x) + v_0 \cos\theta + \gamma(t) \tag{49}$$

and

$$\frac{dy}{dt} = \xi^{-1} V_0 k_0 \cos(k_0 y) + v_0 \sin\theta + \gamma(t), \tag{50}$$

where $\gamma(t) = \Gamma/\xi$. Nevertheless, such a landscape could be implemented experimentally using optical forces. For example, mutually incoherent pairs of laser beams intersecting at right angles would lead to a potential of the form given in Eq. (48), as would pairs with orthogonal polarization.

Since the motions in the $\hat{x}$ and $\hat{y}$ directions are independent in this case, the same exponential sensitivity to particle size, Eq. (32), is obtained, in the absence of thermal forces. As well, the same integration can be used to determine the average deflection angle for free-flowing particles, analogous to Eq. (38):

$$\tan\psi = \frac{\sqrt{\sin^2\theta - \eta^2}}{\sqrt{\cos^2\theta - \eta^2}}. \tag{51}$$

Similarly, for finite temperatures, the mean deflection angle is given by

$$\tan\psi = \tan\theta \frac{1 + [(2\sin\theta)/\eta]\,\mathrm{Im}[S_1(\tau, \sin\theta/\eta)]}{1 + [(2\cos\theta)/\eta]\,\mathrm{Im}[S_1(\tau, \cos\theta/\eta)]}. \tag{52}$$

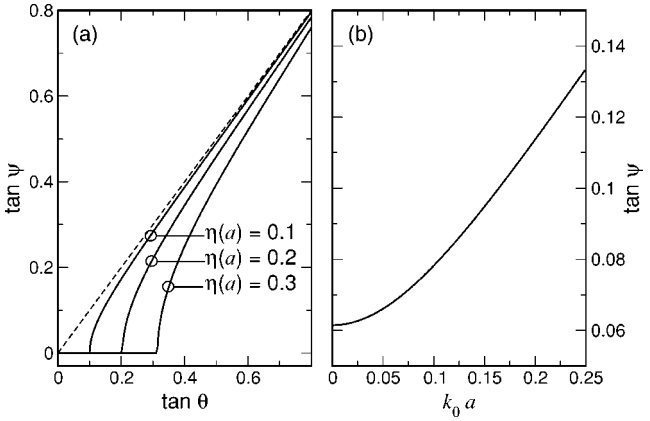

FIG. 5. (a) Deflection as a function of orientation for a separable two-dimensionally modulated landscape at $\eta(a) = 0.1$, 0.2, and 0.3. The diagonal dashed line indicates the result with no landscape. (b) Size dependence of the deflection angle for $\eta_0 = 0.4$ and $\tan\theta = 0.441$.

The zero-temperature deflection angle is plotted in Fig. 5 as a function of the angle θ of the driving force, for a fixed value of the normalized potential η. Also plotted is ψ as a function of particle size a for a fixed θ. The results can be seen to be similar to those obtained with one-dimensional fringes. In other words, no qualitative difference is obtained in this case by modulating in two directions rather than just one.

In order to see other effects of increased dimensionality, it is necessary to consider landscapes that cannot be separated into one-dimensional terms; i.e., landscapes where the motion in one dimension depends on the position in the other. Analytical solutions are not available for such landscapes. However, it is possible to develop limiting arguments that illustrate some novel features of transport in such landscapes, including the continued possibility for sorting that is exponentially sensitive to particle size.

VI. LINEAR TRAP ARRAYS

A. Periodically modulated fringe

Combining aspects of Secs. III and IV, we next consider landscapes that are featureless outside a bounded region in the $\hat{y}$ direction, and are periodically modulated in the $\hat{x}$ direction. This features the clean separations of the continuous barrier with the exponential selectivity of sinusoidal landscapes. It also provides a straightforward example of the surprising complexity of nonseparable landscapes.

The simplest exemplar is the modulated line

$$I(\mathbf{r}) = I_0\, A(y) \frac{1 + s\cos(k_0 x)}{1 + s}, \tag{53}$$

where $A(y)$ describes the transverse profile and is peaked at $A(0) = 1$. Here, the factor s controls the depth of modulation along the line and falls in the range $0 < s < 1$. Such an array can be realized, for example, with a linear array of discrete optical tweezers. Choosing $s > 1$ would correspond to alternating potential wells and barriers, which also could be

implemented optically, for instance with two different wavelengths of light.

At a given driving orientation θ, objects either are locked in to the array and deflected, or else escape into the driving direction. This is unlike the sinusoidal landscape, for which even the particles that are not locked in are deflected away from the driving direction. Collection of the desired fraction should thus be more straightforward for the linear array of traps.

The equations of motion for objects driven deterministically through $I(\mathbf{r})$ at angle θ are

$$\frac{dx}{dt} = \xi^{-1} F_x(\mathbf{r}) + v_0 \cos\theta \tag{54}$$

and

$$\frac{dy}{dt} = \xi^{-1} F_y(\mathbf{r}) + v_0 \sin\theta, \tag{55}$$

where the components of the substrate-mediated force reflect a convolution with a particle's form factor. We will assume the particles' form factors to be separable, as in Eq. (14), thereby sacrificing some generality in favor of clarity, so that

$$F_x(\mathbf{r}) = \alpha I_0 k_0 a^2 \overline{A}(y) \frac{s\tilde{f}_x(k_0 a)\sin(k_0 x)}{1+s} \tag{56}$$

and

$$F_y(\mathbf{r}) = -\alpha I_0 a^2 \partial_y \overline{A}(y) \frac{1+s\tilde{f}_x(k_0 a)\cos(k_0 x)}{1+s}, \tag{57}$$

where the effective transverse profile is $\overline{A}(y) = (f_y \circ A)(y)$. Even this simplified set of coupled equations is highly nonlinear and cannot be integrated directly. Instead, we resort to limiting arguments to determine when particles become locked in and when they escape. These estimates provide the basis for our claim that sorting by inclined arrays of traps or barriers can offer exponential size selectivity.

As for the uniform fringe in Sec. III, the restoring force $F_y(\mathbf{r})$ attains its maximum value along $y = y_{\max}$, with $y_{\max} > 0$ for attractive wells and $y_{\max} < 0$ for repulsive barriers. For this separable model, $y_{\max}$is a solution to $\partial_y^2 \overline{A}(y) = 0$. In more general nonseparable systems, it varies with position x along the array. In either case, this threshold depends on the object's geometry and composition through the form factor $f(\mathbf{r})$.

A particle's trajectory must cross $y = y_{\max}$ if it is to escape the line of traps. This requires there to be at least some points x along the array where $F_0 \sin\theta > F_y(x, y_{\max})$. Limits on this condition can easily be established, with

$$F_0 \sin\theta \geqslant \max_x \{F_y(x, y_{\max})\} \tag{58}$$

ensuring that every trajectory escapes and

$$F_0 \sin\theta \geqslant \min_x \{F_y(x, y_{\max})\} \tag{59}$$

opening up the possibility that at least some trajectories might. The associated bounds on θ_m, the marginally locked-in angle, are

$$\eta(a)\frac{1 - s\tilde{f}_x(k_0 a)}{1+s} < \sin\theta_m < \eta(a)\frac{1 + s\tilde{f}_x(k_0 a)}{1+s}, \tag{60}$$

where $\eta(a) = \alpha k_0 a^2 \overline{A}(y_{\max})/F_0$. With this definition, $\eta(a)$ depends only weakly on a, as in Sec. III.

The limit of weak modulation, $s = 0$, once again yields Eq. (23), the result for a continuous barrier or trench. Similarly, since $\lim_{a\to\infty} \tilde{f}_x(k_0 a) = 0$, large particles with $k_0 a > 1$ are not significantly affected by the modulation. Smaller particles encountering a deeply modulated line, $s \to 1$, are more interesting. Unfortunately, the simple bounds in Eq. (60) have no predictive power in this range, because $\lim_{a\to 0} \tilde{f}_x(k_0 a) = 1$ and Eq. (60) reduces to $0 < \sin\theta_m < \eta(a)$.

This is not to say that exponential selectivity is lost in this range, but rather that a more detailed analysis is required to ascertain when it can be attained. To illustrate the possibility of achieving exponential sensitivity, we consider an experimentally realizable landscape consisting of a line of discrete optical tweezers [6], which we model as a line of discrete Gaussian wells.

B. Line of Gaussian wells

After convolution with a Gaussian form factor, a single well of intrinsic width w takes the form

$$V_1(\mathbf{r}) = -V_0 \exp\left(-\frac{r^2}{2\sigma^2}\right) \tag{61}$$

with $\sigma^2(a) = w^2 + a^2$. This should not be mistaken for an accurate model of an optical tweezer's potential well, but rather as a tractable model whose behavior approximates that observed in actual optical traps. A line of such wells separated by a distance b results in the potential-energy landscape

$$V(\mathbf{r}) = V_0(a) \sum_n \exp\left(-\frac{(\mathbf{r} - nb\hat{x})^2}{2\sigma^2(a)}\right). \tag{62}$$

Any trajectory locked in to this periodic landscape will itself be periodic in x. This means that such a trajectory passes through a sequence of turning points at which $\partial_x y(x,t) = \partial_t y(x,t) = 0$. Any trajectory lacking such turning points cannot be locked in, and so must escape from the line of potential wells. Turning points come in two varieties: those where particles make their nearest approaches to the wells' centers, and those corresponding to their furthest excursions from the line of traps. Particles can escape when the latter type disappear.

For small to moderate driving angles θ, the more distant turning points occur near the midplanes between traps, where the restoring force is weakest. Considering the influence of just two traps (appropriate for $b > \sigma$), centered at $x = 0$ and $x = b$, this suggests the point of escape will be near $x = b/2$

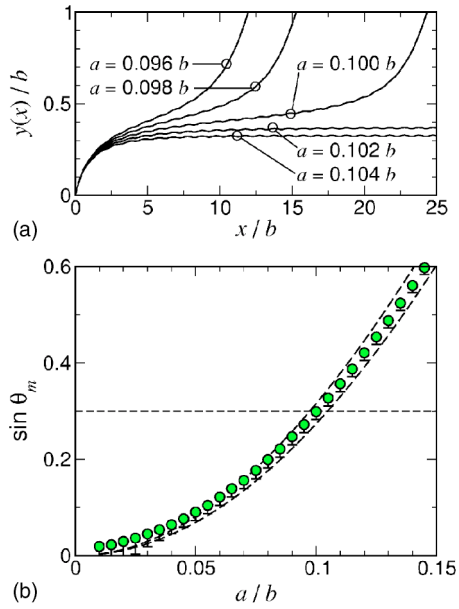

FIG. 6. (a) Trajectories calculated according to Eqs. (54) and (55) for the line of Gaussian wells described by Eq. (62). The wells are separated by distance b and have intrinsic width $w=0.4b$. Their effective width is $\sigma=\sqrt{w^2+a^2}$, where a is the radius of a sphere flowing through the array. The effective potential well depth is $\eta(a)=(2/\sqrt{e})V_0/(\sigma F_0)=9.7\ \sigma^2/a^2$. With the driving force oriented at $\theta=17.5^\circ$, spheres with radii larger than $a=0.1b$ are locked into the line. (b) Dependence of the marginally locked-in deflection angle θ_m on radius, a. The lower dashed curve is the prediction of Eq. (63) and the upper from Eq. (60). The horizontal dashed line indicates the orientation along which the data in (a) were calculated.

and $y=\sigma$. Expanding around this point yields

$$\sin\theta_m \lesssim \eta(a)\exp\left(-\frac{b^2}{8\sigma^2}\right), \tag{63}$$

where $\eta(a)=(2/\sqrt{e})V_0/(\sigma F_0)$ measures the traps' strength relative to the driving force. Because Eq. (63) is an upper bound, no locked-in trajectories can occur for $\theta>\theta_m$. Equation (63) therefore establishes the exponential size dependence of particle deflection.

Figure 6 shows results of numerical simulations of transport across a line of Gaussian potential wells. These simulations were designed to model the experimental design of Ref. [6], in which colloidal spheres are driven by flowing fluid past an inclined line of discrete optical traps. The driving force for this system is $F_0\approx\xi a u$, where ξ is the viscous drag coefficient corrected for hydrodynamic coupling to walls, a is the radius, and u is the flow speed. The sample trajectories in Fig. 6(a) were calculated for $w=0.4\,b$ and $\eta(a)=9.7\ \sigma^2/a^2$ at a fixed orientation of $\theta=17.5°$. They demonstrate that spheres with radii larger than $a=0.1\ b$ are locked in to the array of traps under these conditions, while smaller spheres escape. Even a comparatively short array can resolve differences in radius of just a few percent, suggesting that nanometer-scale resolution should be attainable for hundred-nanometer-scale spheres in practical optical implementations.

Figure 6(b) shows how the marginally locked-in angle varies with size for this array. The lower dashed curve in Fig. 6 is the prediction of Eq. (63). Its very good agreement with simulation results in this parameter range confirms that the limiting argument establishes a useful lower bound on the θ_m. These results therefore confirm that fractionation by a line of traps offers exceptional size selectivity in an appropriate range of conditions. Figure 6(b) also demonstrates that the locked-in fraction can be deflected to large angles, contrary to assertions in previous reports [5].

While $b>\sigma$ ensures optical fractionation's exponential size selectivity, other considerations provide a basis for optimizing the intertrap separation. The total lateral deflection for a captured particle in an N-trap array is $(N-1)b\sin\theta$. The array's efficiency can be defined accordingly as the lateral deflection per trap: $\Delta(a,b)=b\sin\theta$. Choosing $b=2\sigma(a)$ optimizes this efficiency at $\Delta=(4/e)V_0/F_j$. This result, however, does not necessarily optimize sensitivity to particle size.

The sensitivity may be formulated as

$$S(a,b)\equiv\frac{\partial\Delta(a,b)}{\partial a}, \tag{64}$$

and is optimized by setting

$$\frac{\partial S(a,b)}{\partial b}=\frac{\partial^2\Delta(a,b)}{\partial b\,\partial a}=0. \tag{65}$$

This yields an optimal separation somewhat larger than that for maximum deflection:

$$\frac{b^2}{4\sigma^2}=1+\chi(a)+\sqrt{3+\chi^2(a)}, \tag{66}$$

with

$$\chi(a)=\frac{1}{2}\left[1-\frac{\eta'(a)}{\eta(a)}\frac{\sigma(a)}{\sigma'(a)}\right]. \tag{67}$$

Although fractionation by a line of optical traps has been demonstrated in practice [6], optimization based on these criteria has yet to be implemented.

VII. CONCLUSIONS

Periodic potential-energy landscapes have exceptional promise for sorting continuous streams of mesoscopic objects. Whether an object becomes locked in to a symmetry-selected direction through the landscape or instead follows the direction of the driving force can depend sensitively on size. This can be shown quite generally for the separable potentials considered in Secs. IV and V. More subtle landscapes, which involve coupled motions in two or more dimensions, are more difficult to analyze. Approximate arguments and simulations show that a particular one of these, a line of Gaussian wells, offers both exponential size selectivity and clean binary separations. More sophisticated, nonseparable, higher-dimensional landscapes, such as two-dimensional arrays of optical traps [4], optical lattices [5], and microfabricated post arrays [2,3], can distribute continu-

ous distributions of objects into discrete fractions [28]. The analysis in this case is made far more difficult by the lack of closed-form solutions to the equations of motion, even in the deterministic limit.

Randomization by thermal forces substantially degrades the selectivity with which a one-dimensionally modulated landscape can retain objects. A related study demonstrates that thermal forcing restructures the pattern of locked-in states in a two-dimensional array of potential wells [28], and eventually wipes them out as the array grows in size. This contradicts the assertion [5] that thermally assisted hopping can lead to exponential size selectivity. Fortunately, the sorting processes discussed here, as well as their generalizations, can be driven into the deterministic limit by increasing the driving and trapping forces.

Continuous, continuously tuned chromatographic size separations should have many applications in biological research, drug discovery, and purification of mesoscale materials. This article outlines the basic principles by which they work, and suggests considerations for their optimization for particular applications.

ACKNOWLEDGMENTS

This work was supported by the National Science Foundation under Grants No. DBI-0233971 and No. DMR-0304906.

[1] H. Risken, *The Fokker-Planck Equation*, 2nd ed (Springer-Verlag, Berlin, 1989).
[2] T. A. J. Duke and R. H. Austin, Phys. Rev. Lett. **80**, 1552 (1997).
[3] L. R. Huang, E. C. Cox, R. H. Austin, and J. C. Sturm, Science **304**, 987 (2004).
[4] P. T. Korda, M. B. Taylor, and D. G. Grier, Phys. Rev. Lett. **89**, 128301 (2002).
[5] M. P. MacDonald, G. C. Spalding, and K. Dholakia, Nature (London) **426**, 421 (2003).
[6] K. Ladavac, K. Kasza, and D. G. Grier, Phys. Rev. E **70**, 010901 (2004).
[7] D. A. McQuarrie, *Statistical Mechanics* (University Science Books, Mill Valley, CA, 2000).
[8] *Encyclopedia of Separation Science*, edited by I. D. Wilson, (Academic Press, San Diego, 2000).
[9] J. Wiersig and K.-H. Ahn, Phys. Rev. Lett. **87**, 026803 (2001).
[10] C. Reichhardt and F. Nori Phys. Rev. Lett. **82**, 414 (1999).
[11] C. Reichhardt and G. T. Zimányi, Phys. Rev. B **61**, 14354 (2000).
[12] C. Reichhardt, R. T. Scalettar, G. T. Zimányi, and N. Grønbech-Jensen, Phys. Rev. B **61**, R11914 (2000).
[13] V. I. Marconi and D. Domínguez, Phys. Rev. B **63**, 174509 (2001).
[14] O. Pierre-Louis and M. I. Haftel, Phys. Rev. Lett. **87**, 048701 (2001).
[15] C. F. Chou, R. H. Austin, O. Bakajin, J. O. Tegenfeldt, J. A. Castelino, S. S. Chan, E. C. Cox, H. Craighead, N. Darnton, T. Duke, J. Y. Han, and S. Turner, Electrophoresis **21**, 81 (2000).
[16] B. H. Weigl and P. Yager, Science **283**, 346 (1999).
[17] W. D. Volkmuth and R. H. Austin, Nature (London) **358**, 600 (1992).
[18] J. Rousselet, L. Salome, A. Ajdari, and J. Prost, Nature (London) **370**, 446 (1994).
[19] L. Gorre-Talini, J. P. Spatz, and P. Silberzan, Chaos **8**, 650 (1998).
[20] A. Ashkin, J. M. Dziedzic, J. E. Bjorkholm, and S. Chu, Opt. Lett. **11**, 288 (1986).
[21] E. R. Dufresne and D. G. Grier, Rev. Sci. Instrum. **69**, 1974 (1998).
[22] E. R. Dufresne, G. C. Spalding, M. T. Dearing, S. A. Sheets, and D. G. Grier, Rev. Sci. Instrum. **72**, 1810 (2001).
[23] J. E. Curtis, B. A. Koss, and D. G. Grier, Opt. Commun. **207**, 169 (2002).
[24] P. C. Mogensen and J. Glückstad, Opt. Commun. **175**, 75 (2000).
[25] C. F. Bohren and D. R. Huffman, *Absorption and Scattering of Light by Small Particles* (Wiley Interscience, New York, 1983).
[26] P. A. Maia Neto and H. M. Nussenzveig, Europhys. Lett. **50**, 702 (2000).
[27] A. E. Chiou, W. Wang, G. J. Sonek, J. Hong, and M. W. Berns, Opt. Commun. **133**, 7 (1997).
[28] A. Gopinathan and D. G. Grier, Phys. Rev. Lett. **92**, 130602 (2004).